



UNIVERSITY OF LEEDS

This is a repository copy of *ATF-2 and Tpl2 regulation of endothelial cell cycle progression and apoptosis*.

White Rose Research Online URL for this paper:
<http://eprints.whiterose.ac.uk/154696/>

Version: Accepted Version

Article:

Fearnley, GW, Latham, AM, Hollstein, M et al. (2 more authors) (2020) ATF-2 and Tpl2 regulation of endothelial cell cycle progression and apoptosis. *Cellular Signalling*, 66. 109481. ISSN 0898-6568

<https://doi.org/10.1016/j.cellsig.2019.109481>

© 2019 Elsevier Inc. All rights reserved. This manuscript version is made available under the CC-BY-NC-ND 4.0 license <http://creativecommons.org/licenses/by-nc-nd/4.0/>.

Reuse

This article is distributed under the terms of the Creative Commons Attribution-NonCommercial-NoDerivs (CC BY-NC-ND) licence. This licence only allows you to download this work and share it with others as long as you credit the authors, but you can't change the article in any way or use it commercially. More information and the full terms of the licence here: <https://creativecommons.org/licenses/>

Takedown

If you consider content in White Rose Research Online to be in breach of UK law, please notify us by emailing eprints@whiterose.ac.uk including the URL of the record and the reason for the withdrawal request.



eprints@whiterose.ac.uk
<https://eprints.whiterose.ac.uk/>

1 **ATF-2 and Tpl2 regulation of endothelial cell cycle**
2 **progression and apoptosis**

3
4
5 Gareth W. Fearnley¹, Antony M. Latham¹, Monica Hollstein², Adam F.
6 Odell^{3,4}, Sreenivasan Ponnambalam^{1*}

7
8
9
10
11 ¹School of Molecular & Cellular Biology, University of Leeds, UK;

12 ²Faculty of Medicine & Health, University of Leeds, UK;

13 ³Leeds Institute of Medical Research at St James's, University of Leeds, UK;

14 ⁴School of Health Sciences, York St. John University, Lord Mayor's Walk, York,
15 UK.

16
17 **Author for correspondence:**

18 Dr Sreenivasan Ponnambalam

19 Endothelial Cell Biology Unit

20 School of Molecular & Cellular Biology

21 University of Leeds

22 Leeds LS2 9JT, UK.

23 Email: s.ponnambalam@leeds.ac.uk

27 **ABSTRACT**

28 Cells respond to soluble and membrane-bound factors to activate signalling
29 cascades that control cell proliferation and cell death. Vascular endothelial
30 growth factor A (VEGF-A) is a soluble ligand that modulates a variety of cellular
31 responses including cell proliferation and apoptosis. It is not well understood
32 how VEGF-A signalling pathways regulate cell proliferation and cell death. To
33 address this, we examined VEGF-A-regulated signalling pathways in the
34 cytosol and nucleus and functional requirement for such cellular responses.
35 The VEGF-A-regulated transcription factor, ATF-2, is required for cell cycle
36 proteins such as p53, p21 and Cyclin D1. A cytosolic serine/threonine protein
37 kinase (Tpl2) modulates ATF-2-regulated effects on the endothelial cell cycle.
38 Such regulatory effects impact on endothelial cell proliferation, cell viability and
39 apoptosis. These cellular effects influence complex cell-based organisation
40 such as endothelial tubulogenesis. Our study now provides a framework for
41 incorporating VEGF-A-stimulated signalling events from the cytosol to the
42 nucleus which helps to understand how cell proliferation and apoptosis are
43 controlled.

44 ***(158 words)***

45

46 ***Keywords:*** Signal transduction, Cell proliferation, Apoptosis, ATF-2, p53, Tpl2

47

48 **1. Introduction**

49 Eukaryote organisms sense changes in the extracellular environment
50 and modulate signal transduction pathways that control different aspects of cell
51 physiology and animal function. An important feature of cellular physiology is
52 to tightly regulate cell proliferation and programmed cell death (apoptosis). One
53 question is how membrane receptors bind extracellular ligands and trigger
54 such signalling pathways that modulate cell proliferation and apoptosis [1]. In
55 higher eukaryotes, a wide variety of membrane receptors exist with ubiquitous
56 and tissue-specific regulatory functions. One such class of proteins are the
57 receptor tyrosine kinase (RTK) family which bind extracellular ligands and
58 transduce signals into the cellular interior, thus modulating cell behaviour and
59 function [2, 3]. It is well known that the RTK activation modulates cell cycle
60 progression in a wide variety of cells and tissues. RTKs are thus useful models
61 to better understand how complex eukaryotes integrate signalling pathways
62 with cell cycle progression and apoptosis.

63 The vascular endothelial growth factor receptor (VEGF) family binds to a
64 subset of receptor tyrosine kinases (VEGFRs) and have provided valuable
65 insights into vascular physiology in health and disease states [4, 5]. The
66 founding member of the VEGF family (i.e. VEGF-A) binds to the pro-angiogenic
67 receptor, VEGFR2, to regulate many aspects of endothelial function including
68 cell migration, proliferation and angiogenesis [6]. The role of VEGF-A and
69 VEGFR2 in promoting signal transduction which impacts on cell migration and
70 endothelial tubule formation (tubulogenesis) is well-characterised. However,
71 the effect of VEGF-A on endothelial cell proliferation although clear-cut, is
72 relatively mild. Interestingly, VEGF-A regulates both cell cycle progression and
73 metabolic control, indicating an ability to simultaneously modulate different
74 biochemical pathways [7].

75 To answer how VEGF-A regulates biochemical events that contributes to
76 choices between cell proliferation and apoptosis, we examined the functional

77 roles of components of signalling pathways regulated by VEGF-A. Different
78 studies have identified both cytosolic and nuclear proteins that regulate VEGF-
79 A-stimulated signal transduction, metabolism and gene expression [6, 8]. We
80 focused on the link between the proto-oncogene and serine/threonine protein
81 kinase, Tpl2 (MAP3K8), the tumour suppressor and cell cycle regulator, p53,
82 and the nuclear transcription factor, ATF-2. Our findings in this study link Tpl2-
83 regulated signal transduction impacting on ATF-2 and p53 levels to regulate
84 cell proliferation and apoptosis which impacts on endothelial tubulogenesis.

85 **2. Materials and Methods**

86 *2.1. Materials*

87 Antibodies used in this study are goat anti-VEGFR2 (R&D Systems,
88 Minneapolis, USA), mouse anti-Cyclin D1 (DCS6), mouse anti-p21, rabbit anti-
89 ATF-2, rabbit anti-phospho-ATF-2 (pT71), rabbit anti-cleaved and total
90 caspase 3, rabbit anti-phospho-VEGFR2-Y1175 (pY1175) (Cell Signaling
91 Technology, Danvers, USA), mouse anti-p53, mouse anti-Cyclin A2, mouse
92 anti-Bax, mouse anti-Cyclin B (BD Transduction Laboratories, Oxford, UK),
93 mouse anti- α -tubulin, mouse anti-actin (Sigma-Aldrich, Poole, UK). Endothelial
94 cell growth medium (ECGM) and recombinant human VEGF-A₁₆₅ and VEGF-
95 A₁₂₁ were from PromoCell (Heidelberg, Germany).

96

97 *2.2. Immunoblotting and analysis*

98 Human umbilical vein endothelial cells (HUVECs) were cultured and
99 grown as previously described [9]. Cells were seeded into 6-well plates until
100 ~80% confluent, cells were washed twice with PBS and starved overnight in
101 MCDB131 + 0.2% (w/v) BSA and 2 mM thymidine, to stimulate cell cycle arrest
102 (G1/S). Starvation media was aspirated and cells stimulated in ECGM + 25 μ M
103 2-deoxycytidine, containing (0.25 nM) VEGF-A₁₆₅ or VEGF-A₁₂₁ if required.
104 Cells were then lysed and processed for immunoblot analysis as previously
105 described [10]. Membranes were imaged using a G:BOX XT4 Chemi imaging
106 system (Syngene, Cambridge, UK). Band intensity was determined using 2-D
107 densitometry running on dedicated image analysis software (Syngene).

108

109 *2.3. Quantitative real-time PCR analysis*

110 HUVECs were subjected to control or ATF-specific siRNA duplex
111 treatments as previously described. Cells were then starved for 2 h in minimal

112 media, before stimulation with VEGF-A (25 ng/ml) for 2 h followed by cell lysis
113 and processing for qRT-PCR analysis. Total cellular RNA was reverse
114 transcribed into cDNA using random hexamer primers included in the High-
115 Capacity cDNA Archive Kit (Life Technologies) [11]. PCR reactions were
116 performed in a LightCycler apparatus using the LC-FastStart DNA Master
117 SYBR Green I kit (Roche Diagnostics, Mannheim, Germany) as described
118 previously [12]. 2 µg of total RNA were used for first-strand cDNA synthesis
119 with Superscript II reverse transcriptase and oligo d(T)12–18 primers according
120 to the manufacturer's protocol (Life Technologies). Primer sequences used for
121 qRT-PCR are: human Tpl2 forward primer: 5'- CGC AAG AGG CTG AGT A-3'
122 and human Tpl2 reverse primer: 5'-TTC CTG TGC ACG AAG AAT CA-3'. All
123 PCR reactions were optimised at the same annealing temperature of 60°C and
124 thermocycling for each reaction was subsequently performed in a final volume
125 of 20 µl containing 2 µl of cDNA sample, 4 mM MgCl₂, 0.5 µM of each primer
126 and 2 µl of LC-FastStart DNA Master SYBR Green I. Samples were initially
127 denatured for 8 min at 95°C, followed by 45 cycles of denaturation (95°C for
128 15 sec), annealing (60°C for 5 sec), elongation (72°C for 10 sec), and a short
129 temperature increase to 82°C for 3 sec (for fluorescence measurements). PCR
130 products were quantified relative to a housekeeping gene encoding β-actin.
131 Expression levels of all other genes are given relative to the expression levels
132 of β-actin by evaluation of their crossing-over points of product accumulation
133 curves relative to the standard curve of β-actin. All PCR products were checked
134 by melting point analysis and by agarose gel electrophoresis to verify that
135 products were of correct length.

136

137 *2.4. Fucci immunofluorescence analysis*

138 The fluorescent ubiquitinated cell cycle indicator (Fucci) has been
139 previously described [13]. Briefly, a novel puromycin-resistant single co-

140 expression construct was generated as follows. Plasmid pLV-eGFP (Addgene
141 #36083; a gift from Pantelis Tsoulfas) was digested with BamHI and Sall to
142 remove the eGFP open reading frame. PCR primers were used to amplify
143 sequences encoding mKO2-hCdt1 (30/120) (5'-TAG AAG ACA CCG ACT
144 CTA GAG GAT CCA TGG TGA GTG TGA TTA AAC-3' and 5'-ACG TCG CCG
145 CAG GTC AGC AGG CTG CCT CTG CCC TCG CCG CTG CCG ATG GTG
146 TCC TGG TCC TGC GC-3') and mAG-hGem (1/110) (5'-CAG CCT GCT GAC
147 CTG CGG CGA CGT GGA GAA CCC CGG CCC CGT GAG CGT GAT CAA
148 GCC CGA G-3' and 5'-ACG TCT CCA CAT GTC AGG CTT CCT CTT CCT
149 TCT CCG CTT CCC AGC GCC TTT CTC CGT TTT TCT G-3'), and Pac (5'-
150 AAG CCT GAC ATG TGG AGA CGT GGA AGA AAA CCC TGG GCC CGC
151 CAC CGA GTA CAA GCC CAC G-3' and 5'-TAA TCC AGA GGT TGA TTG
152 GCT AGC TCA GGC ACC GGG CTT GCG GGT C-3'), from the FUCCI
153 plasmid templates [13] and pGIPZ, respectively. Gibson assembly was used to
154 create pLV-FUCCI, which encodes a T2A peptide linking mKO2-hCdt1
155 (30/120) with mAG-hGem (1/110), and a P2A peptide linking mAG-hGem
156 (1/110) with Pac. To overcome difficulties caused by high GC-content in
157 overlapping regions, the three inserts were joined using splicing by overlap
158 extension (2) before addition to the assembly reaction. Supernatants
159 containing lentiviral particles were generated in HEK293T cells using a 3rd
160 generation packaging system obtained from Addgene. Endothelial cells were
161 incubated with lentivirus carrying the FUCCI reporter and a puromycin marker
162 and cultured for up to 3-4 weeks in ECGM containing puromycin (3 µg/ml).

163 Following transduction with high-titre viral solutions generated in
164 HEK293T cells, endothelial cells were transfected with specific siRNA duplexes
165 for 48 h prior to being starved overnight in MCDB131 + 0.2% (w/v) BSA and 2
166 mM thymidine (G1/S cell cycle arrest). Cells were subsequently trypsinised and
167 reseeded into 96-well, black-walled plates at 2.5×10^3 cells per well in ECGM +
168 25 µM 2-deoxycytidine and imaged at 8 h and 30 h post release following

169 addition of Hoechst 33342 to visualise nuclear DNA. Image acquisition was
170 carried out using either a BD Pathway 435 imager or Olympus X81
171 immunofluorescence microscope equipped with 405 nm, 488 nm, and 543 nm
172 light-source lines. Image analysis was performed using ImageJ and
173 Metamorph 6 software (Universal Imaging, Media, PA) on between 400-2000
174 cells at each time-point per siRNA duplex treatment.

175

176 *2.5. Cell viability assays*

177 3000 HUVECs were seeded per well of a 96-well plate, cultured in 90 μ l
178 ECGM for 16-20 h, before adding 10 μ l of MTS reagent (CellTiter 96 AQueous
179 Non-Radioactive Cell Proliferation Assay, Promega, Madison, USA). After
180 further incubation for 4 h, colour change caused by reduction of the yellow
181 tetrazolium compound (MTS) by metabolically active cells to brown formazan
182 was monitored at 490 nm using a Tecan Sunrise plate reader (Mannedorf,
183 Switzerland).

184

185 *2.6. Annexin V apoptosis assay*

186 20000 HUVECs were seeded into 24-well plates and left overnight for
187 16-20 h. Media was removed and cells were subjected to RNAi and protein
188 knockdown as previously described. Cells were gently detached from the
189 substratum using previously described protocol for processing for flow
190 cytometry. Before this was carried out, cells were centrifuged at 1000 g for 5
191 mins and resuspended in 0.5 ml of Annexin V binding buffer using a kit (Sigma-
192 Aldrich, Poole, UK). Annexin V-FITC conjugate (to stain apoptotic cells) and
193 propidium iodide (to stain DNA of dead or dying cells) was added as
194 recommended by manufacturer. Samples were then examined using a
195 Fortessa flow cytometer (Becton Dickinson, UK) and >10000 labelled cells

196 were analysed per experiment. Early apoptotic cells show labelling with the
197 Annexin V-FITC conjugate alone. Live cells show no labelling with either the
198 propidium iodide or Annexin V-FITC. Necrotic cells are labelled by both
199 propidium iodide and Annexin V-FITC.

200

201 *2.7. Cell proliferation assay*

202 2000 HUVECs were seeded per well of a 96-well plate and left overnight
203 for 16-20 h. Media was removed and replaced with serum-free medium for 3 h,
204 then stimulated with 0.25 nM VEGF-A in 100 μ l for 24 h. 10 μ M BrdU was
205 added per well at this point. Cell proliferation ELISA was used according to
206 manufacturer's protocol (Roche Diagnostics, Mannheim, Germany). Colour
207 change was developed using 3,3',5,5'-tetramethylbenzidine solution and the
208 reaction quenched with 1 M H₂SO₄. Absorbance was measured at 450 nm
209 using a variable wavelength Tecan Sunrise plate reader (Tecan, Mannedorf,
210 Switzerland).

211

212 *2.8. Tubulogenesis assay*

213 Primary human foreskin fibroblasts (Promocell) were cultured in 48-well
214 plates until confluent, before seeding 7500 endothelial cells per well onto the
215 fibroblast monolayer and left overnight for 20-24 h essentially as previously
216 described [9]. Briefly, media was aspirated and replaced with fresh media
217 supplemented with VEGF-A (0.25 nM) every 2-3 days for 7 days. Co-cultures
218 were fixed in 200 μ l 10% (v/v) formalin for 20 min at room temperature,
219 quenched and labelled with mouse anti-human PECAM-1 (CD31) and donkey
220 anti-mouse Alexa Fluor 594 conjugate as previously described [9]. Processed
221 samples containing stained endothelial tubules were visualized using an
222 EVOS-fl inverted digital microscope (ThermoFisher). 3 random fields were
223 imaged per well. Total tubule length was then quantified from each

224 photographic field using the open source software AngioQuant
225 (www.cs.tut.fi/sgn/csb/angioquant) and values averaged. For a more detailed
226 methods see elsewhere [9].

227

228 *2.9. Statistics*

229 We used one-way analysis of variance (ANOVA) followed by Tukey's
230 post-hoc test or two-way ANOVA followed by Bonferroni multiple comparison
231 test using GraphPad Prism software (La Jolla, USA). Significant differences
232 between control and test groups were evaluated with p values less than 0.05
233 (*), 0.01 (**), 0.001 (***) and 0.0001 (****) indicated on the graphs or
234 histograms. Error bars denote mean \pm SEM.

235 **3. Results**

236 *3.1. ATF-2 modulates p21, p53 and Cyclin D1 levels*

237 In primary endothelial cells VEGF-A regulates signal transduction and
238 cell proliferation [14] partially through recruitment of nuclear transcription
239 factors, including c-fos and other AP-1 components [15]. We have previously
240 identified a signalling nexus between VEGFR2, the MAP3K family member
241 Tpl2, and a transcription factor, ATF-2. In previous studies on VEGF-A-
242 stimulated and ATF-2-regulated endothelial gene expression on VCAM-1 [15]
243 and Tpl2 [16], we find that maximal VEGF-A₁₆₅-stimulated, ATF-2-regulated
244 VCAM-1 synthesis occurs 8 h after VEGF-A addition. Under such conditions,
245 there is complexity in decreased VEGFR2 levels caused by increased
246 ubiquitination, endocytosis and degradation [15]. However, there is also a rise
247 in new VEGFR2 synthesis [15], which can also substantially add to VEGFR2
248 activation in the presence of excess exogenous VEGF-A. However, the
249 influence of this pathway on endothelial cell cycle progression and survival was
250 unknown. To ascertain whether different VEGF-A isoforms regulate cytosolic
251 and nuclear signalling events which impact on the endothelial cell cycle, we
252 probed the biochemical state of key regulatory proteins associated with such
253 events (Fig. 1). As previously reported [17], two different VEGF-A isoforms
254 (VEGF-A₁₆₅ and VEGF-A₁₂₁) show differential ability to activate VEGFR2,
255 revealed by varied phospho-VEGFR2 (Y1175) levels (Fig. 1A). Such signalling
256 further impacts on gene expression, as shown by increased levels of VCAM-1
257 in response to VEGF-A₁₆₅ stimulation for 8 h (Fig. 1A). As ATF-2 is implicated
258 in the VEGF-A-stimulated (after 8 h) VCAM-1 increase, concomitant with a
259 decrease in VEGFR2 levels [17], we depleted ATF-2 levels using RNA
260 interference (RNAi) (Fig. 1A, 1B). Knockdown of ATF-2 levels resulted in ~50%
261 decrease in this essential nuclear regulator (Fig. 1B). However, ATF-2
262 knockdown did not affect levels of either Cyclin A2 or Cyclin B, critical drivers
263 of cell proliferation (Fig. 1A). Unexpectedly, depletion of ATF-2 caused

264 elevated levels of two other cell cycle regulators, Cyclin D1 and the cyclin-
265 dependent kinase inhibitor, p21 (Fig. 1A). The latter is a major transcriptional
266 target of the tumour suppressor p53, suggesting p53 involvement in the
267 process.

268 There is link between VEGF-A-stimulated ATF-2 phosphorylation and
269 ATF-2 levels [15, 16]. Activation of the p53 tumour suppressor is known to
270 increase levels of p21, a negative cell cycle regulator, thus potentially
271 impacting additional cell cycle modifiers including Cyclin D1 [18-20]. We
272 explored further links between ATF-2 and p53 by knockdown of either protein
273 alone or together (Fig. 1C). As expected, ATF-2 knockdown abrogated the
274 VEGF-A-stimulated increase in VCAM-1 expression (Fig. 1C, 1D). ATF-2
275 knockdown elevated p21 levels substantially. Importantly, p53 levels were also
276 elevated under such conditions (Fig. 1C, 1E). The >2-fold increase in p53
277 levels caused by ATF-2 knockdown were reversed by p53 or combined ATF-
278 2/p53 knockdown (Fig. 1E). Under these conditions, ATF-2 knockdown caused
279 ~3.5-fold rise in Cyclin D1 levels (Fig. 1F). Furthermore, the increased p21 and
280 cyclin D1 expression evident upon ATF-2 depletion were dependent on the
281 presence of p53, as co-depletion of ATF-2 and p53 abolished the increases
282 (Fig. 1C-F). However, VCAM1 levels were not rescued by depletion of both
283 ATF-2 and p53 (Fig. 1D).

284

285 *3.2. Tpl2 dependence on ATF-2 and impact on p53 and Cyclin D1*

286 The MAP3K family member and oncoprotein, Tpl2, which is implicated in
287 lung carcinogenesis [21] regulates VEGF-A-stimulated angiogenesis [22] and
288 transduces signals from the cytosol to the nucleus in endothelial cells [16]. To
289 assess whether Tpl2 is functionally linked to levels of ATF-2 and cell cycle
290 regulators such as p53, we asked whether RNAi altered protein expression
291 (Fig. 2A). Knockdown of Tpl2 caused ~60% reduction in protein levels (Fig.

292 2B). Tpl2 depletion also suppressed ATF-2 expression to levels similar to those
293 observed after direct ATF-2 knockdown (Fig. 2A). Surprisingly, although ATF-
294 2 knockdown caused >2-fold increase in p53, and Tpl2 depletion also reduced
295 ATF-2 expression, Tpl2 RNAi had no substantial effect on p53, p21, or Cyclin
296 D1 protein levels (Fig. 2A, 2D, 2E). However, combined depletion of both ATF-
297 2 and Tpl2 caused p53 and cyclin D1 protein levels, to return to baseline (Fig.
298 2A, 2D, 2E). Depletion of Tpl2 caused >60% reduction in steady-state Tpl2
299 levels (Fig. 2B).

300 ATF-2 depletion elevates Tpl2 protein expression (Fig. 2A), indicative of
301 a functional link between the two proteins. To explore this further we carried
302 out qRT-PCR to analyse the link between ATF-2 and *Tpl2* expression (Fig. 2C).
303 In a comparison between control and VEGF-A-stimulated conditions, we found
304 ~15-fold increase in *Tpl2* mRNA levels (Fig. 2C). Depletion of ATF-2 levels
305 caused reduction in *Tpl2* mRNA to background levels (Fig. 2C). ATF-2
306 knockdown elevates cell cycle regulator levels (cyclin D1, p53, p21) but Tpl2
307 depletion reverses such effects (Fig. 2D, 2E), suggesting Tpl2 expression is
308 required for mediating the p53 increase evident upon ATF-2 knockdown. The
309 presence of ATF-2 might act as a mitotic accelerator or enabler by dampening
310 the expression of p53 and its downstream cell cycle inhibitors, including p21,
311 via a mechanism dependent on Tpl2 activity.

312 The eukaryote cell cycle is regulated by a combination of protein kinases,
313 cyclins and transcription factors [20, 23, 24]. The previous data in this study
314 suggested that ATF-2 levels influences cell cycle proteins. To assess whether
315 the endothelial cell cycle is affected by ATF-2, we used the fluorescent
316 ubiquitinated cell cycle indicator (FUCCI) [13] which is a dual reporter system
317 used to monitor progression through the cell cycle in living cells, tissues and
318 animals [25]. A lentiviral FUCCI construct was used to transduce primary
319 endothelial cells and cell synchronisation (see Materials and Methods) before
320 monitoring of fluorescent reporter proteins, mKO2-hCdt1 (red) for non-cycling

321 G1 stage cells, and mAG-hGem (green) for proliferating G2/M stage cells
322 (green) (Fig. 3A). Under control conditions, stimulation with VEGF-A caused
323 transient increase in the G1:G2/M ratio after 8 h which is more than 2-fold
324 higher than that that observed after 30 h (Fig. 3B), indicating a rise in the
325 number of cells in G2/M phase within soon after VEGF-A stimulation. Here,
326 depletion of either ATF-2 or p53 had no effect on the G1:G2/M ratio compared
327 to controls (Fig 3B). However, combined ATF-2/p53 caused a significant >2-
328 fold increase in the proportion of cells in G2/M after 30 h (Fig 3B). Furthermore,
329 knockdown of Tpl2 caused a dramatic rise in proportion of cells in the G2/M
330 phase both at the 8 h and 30 h time points (Fig. 3B). However, the relative
331 difference between the 8 h and 30 h time points was a 2-3-fold change in Tpl2-
332 depleted cells, similar to controls (Fig. 3B). Interestingly, combined ATF-2/Tpl2
333 knockdown showed little change between the 8 h and 30 h time points (Fig.
334 3B), suggesting substantial effects on the endothelial cell cycle.

335 Cells that are senescent or have exited the cell cycle are in G0, and p53
336 is a key regulator of cellular senescence [19]. One possibility is that depletion
337 of cell cycle regulatory factors results in increased endothelial cell senescence
338 or cell cycle exit. We evaluated the proportion (%) of the endothelial cell
339 population lacking staining for both mAG and mKO indicative of G0 (Fig. 3C).
340 This was substantially higher in the cells depleted of ATF-2 (Fig. 3C). However,
341 this effect was rescued upon combined knockdown of either ATF-2/p53 or ATF-
342 2/Tpl2 (Fig. 3C). Furthermore, we found that in addition to cell cycle arrest,
343 ATF-2 knockdown also resulted in ~40% decrease in endothelial cell viability
344 (Fig. 3D).

345

346 *3.3. ATF-2, Tpl2 and p53 modulation of apoptosis*

347 One question arising from these data is how endothelial cells integrate
348 complex signal transduction pathways with nuclear gene expression to

349 influence programmed (i.e. apoptosis) and general (i.e. necrosis) cell death. To
350 address this, we used flow cytometry (see Materials and Methods) to identify,
351 necrotic, early and late apoptotic endothelial cell populations (Fig. S1). We
352 used controls (Fig. S1) to evaluate early and late apoptotic cells compared to
353 necrotic cells under conditions of specific protein depletion (Fig. S1B).
354 Quantification of the AnxV-positive population revealed ~4-fold rise in such
355 endothelial cells upon ATF-2 depletion (Fig. 4A). Tpl2 depletion also caused
356 >2-fold rise in AnxV-labelled cell population compared to control (Fig. 4A). A
357 similar profile was observed when the relative cell population was analysed
358 with early apoptotic cell population marked increased >2-fold upon either ATF-
359 2 or Tpl2 depletion (Fig. 4B). In the analysis of late apoptotic cells, ATF-2
360 depletion caused a >4-fold rise in apoptotic cells, and only a ~2-fold rise in Tpl2-
361 depleted cells (Fig. 4C). Considering the total apoptotic cell population, the
362 ATF-2 or Tpl2-depleted cells all show significant 2-3-fold rise in apoptosis (Fig.
363 4D). In these flow cytometry experiments, simultaneous depletion of ATF-
364 2/Tpl2 or ATF-2/p53 causes a reversal in the effects observed with ATF-2
365 depletion alone (Fig. 4A-4D).

366 To explore the molecular basis for increased endothelial apoptosis
367 caused by ATF-2 depletion, we assessed the biochemical status of key
368 apoptotic regulators (Fig. 4E). Immunoblotting of control (scrambled) and ATF-
369 2-depleted endothelial cells revealed an increase in cleaved pro-apoptotic
370 Caspase 3 (Fig. 4E). There were also increased levels of p53 and pro-apoptotic
371 Bax proteins in ATF-2-depleted cells (Fig. 4E). Quantification of these data
372 showed >2-fold rise in cleaved Caspase 3 upon ATF-2 depletion (Fig. 4F).

373

374 *3.4. ATF-2, Tpl2 and p53 involvement in VEGF-A-regulated endothelial cell* 375 *responses*

376 VEGF-A promotes multiple endothelial responses including cell viability,
377 cell proliferation and tubule formation, key features of angiogenesis [4, 5]. We
378 compared endothelial cell viability upon knockdown of specific cytosolic and

379 nuclear factors: ATF-2 knockdown caused ~50% decrease in VEGF-A-
380 stimulated cell viability (Fig. 5A). Tpl2 knockdown also caused ~30% decrease
381 in VEGF-A-stimulated cell viability (Fig. 5A). However, simultaneous combined
382 knockdown of either ATF-2/p53, or ATF-2/Tpl2 caused cell viability to return to
383 baseline levels (Fig. 5A). Depletion of p53 alone had no effect on VEGF-A-
384 stimulated endothelial cell viability (Fig. 5A).

385 As VEGF-A is well-known to stimulate cell proliferation, we asked
386 whether this response was affected by knockdown of components of signal
387 transduction pathways involving ATF-2 and Tpl2 (Fig. 5B). ATF-2 knockdown
388 caused ~30% decrease in endothelial cell proliferation; however, knockdown
389 of p53 or Tpl2 had no effect (Fig. 5B). However, simultaneous knockdown of
390 ATF-2/p53 or ATF-2/Tpl2 returned cell proliferation to control baseline levels
391 (Fig. 5B).

392 One unique feature of VEGF-A is the capacity to stimulate endothelial
393 cells to proliferate, migrate and form biological tubes [26]. We used the *in vitro*
394 endothelial-fibroblast co-culture assay to evaluate VEGF-A-stimulated
395 tubulogenesis (Fig. 5C). VEGF-A stimulation causes ~6-fold increase in
396 average endothelial tubule length under control conditions (Fig. 5D). In
397 contrast, ATF-2 knockdown caused ~50% decrease in endothelial tubule
398 length, (Fig. 5D). Although Tpl2 knockdown caused ~4-fold increase in VEGF-
399 A-stimulated tubule length, there was ~35% reduction in tubulogenesis
400 compared to control (Fig. 5D). Again however, combined knockdown of either
401 ATF-2/p53 or ATF-2/Tpl2 caused return to baseline levels of VEGF-A-
402 stimulated endothelial tubulogenesis (Fig. 5D). Lack of ATF-2 hampers
403 endothelial tubule formation through upregulation of p53 expression and
404 induction of cell cycle arrest, all dependent on the presence of Tpl2.

405

406 **4. Discussion**

407 One important aspect feature of primary cells and tissues is the balance
408 between cell survival, proliferation and different types of cell death. Complex
409 regulatory mechanisms exist to ensure correct timing of cell proliferation in
410 healthy and diseased states. In this study, we investigated how endothelial
411 cells balance cytosolic and nuclear signalling which impacts on cell cycle
412 progression and cell death. Our study suggests a model where Tpl2 receives
413 signals and modulates the activity of downstream factors which regulate gene
414 expression and cell cycle progression (Fig. 6). A balance between Tpl2
415 signalling and ATF-2 nuclear activity is required for normal endothelial
416 responses (Fig. 6A). Reduction in ATF-2 activity impacts on the endothelial
417 commitment to cell cycle progression and apoptosis (Fig. 6B). This function
418 appears dependent on the presence of Tpl2.

419 The evidence for this model is based on 4 lines of evidence. Firstly, ATF-
420 2 depletion promotes a rise in p53, p21 and Cyclin D1 levels, but other cyclins
421 are not affected. This suggests that under such conditions, these endothelial
422 cells have entered a pro-apoptotic phase coincident with cell cycle arrest.
423 Secondly, reduction in ATF-2 levels also causes a rise in the proportion of cell
424 population in senescence (G0), and this coincides with decreased endothelial
425 cell viability. Thirdly, a reduction in Tpl2 levels cause a corresponding decrease
426 in ATF-2 levels, although this was not accompanied by elevated p53, p21, or
427 Cyclin D1 expression, suggesting a functional link between these two proteins,
428 where Tpl2 may be viewed as a master regulator. Importantly, ATF-2 depletion
429 blocks the VEGF-A-stimulated rise in Tpl2 levels, suggesting ATF-2 regulates
430 gene transcription of the *Tpl2* locus. Moreover, loss of ATF-2 is reversed by
431 simultaneous depletion of either Tpl2 or p53, suggesting a regulatory pathway
432 linking all three proteins (Fig. 6). Finally, such regulatory effects are manifested
433 in VEGF-A-stimulated endothelial tubulogenesis, which requires coordination
434 of cell proliferation and migration for biological tube formation. Reduction in

435 ATF-2 levels also reduces the efficiency of endothelial tubulogenesis; however,
436 such effects are reversed by simultaneous depletion of either Tpl2 or p53. This
437 regulatory pathway (Fig. 6) thus impacts on the VEGF-A-stimulated formation
438 of biological tubes.

439 The tumour progression locus 2 (Tpl2/Cot/MAP3K8) gene product was
440 originally identified as a serine/threonine protein kinase in T-cells which
441 regulated signal transduction and cellular responses [27]. Tpl2 is also a proto-
442 oncoprotein, conferring resistance to Raf kinase inhibition [28], promoting
443 breast cancer [29], keratocanthoma and squamous cell carcinoma [30].
444 However, its role in the vascular system is less well-studied, but reports
445 suggest that it can regulate angiogenesis [22] and diabetic retinopathy [31].
446 Our studies now suggest that cytosolic Tpl2 and the nuclear transcription factor
447 ATF-2, are part of a pathway that controls cell cycle progression and apoptosis.
448 The communication between Tpl2 and ATF-2 may occur directly:
449 hyperphosphorylation of ATF-2 is implicated with increased signalling through
450 the MAPK pathway [15]. Recent studies suggest that pharmacological
451 inhibition of p38 MAPK, JNK and AKT signal transduction pathways had little
452 or no effect on ATF-2 phosphorylation in endothelial cells [15]. One possibility
453 is that signalling through the canonical MAPK pathway leads to Tpl2
454 phosphorylation, activation and translocation into the nucleus in a manner
455 analogous to ERK1/2. It has been reported that Tpl2 activity is required for
456 phosphorylation of nuclear factors including ATF-2 [16, 32], implying a
457 functional role in nuclear gene expression. Importantly, a direct nuclear role of
458 Tpl2 has also been reported [30]. This raises the possibility of Tpl2 itself
459 responding to VEGFR2 activation, phosphorylation via canonical (MAPK) or
460 non-canonical pathways which enables nuclear translocation, transcription p
461 factor phosphorylation and modulation of nuclear gene transcription. In
462 endothelial cells, VEGF-A-stimulated signal transduction through a non-
463 canonical signal transduction pathway involving the MEK5-ERK5 axis impacts

464 on a range of vascular responses [33], which could have relevance to Tpl2
465 regulation in this context. In tumour cells, there is evidence that Tpl2 activity is
466 linked to ERK5 status [34].

467 There is a notable relationship between Tpl2 and ATF-2 levels.
468 Decreased Tpl2 levels also cause a substantive decrease in ATF-2 levels;
469 combined ATF-2/Tpl2 knockdown reverses effects caused by ATF-2 depletion
470 alone. However, decreased ATF-2 levels alone, increase Tpl2, p53, cyclin D1
471 and p21 levels; this is not evident when Tpl2 is depleted in isolation, despite
472 ATF-2 levels also falling. Tpl2 expression or activity, appears necessary to
473 allow ATF-2 depletion to stabilise or activate p53, and promote cell cycle arrest.
474 One explanation is that decreased ATF-2 phosphorylation, due to loss of
475 upstream Tpl2, increases post-translational modifications on ATF-2 leading to
476 increased proteolysis and clearance. The loss of ATF-2 leading to increased
477 Tpl2 (Fig. 6B) could be explained by a possible role for ATF-2 in repressing
478 *TPL2* nuclear gene expression. Alternatively, ATF-2 could activate
479 transcription of genes encoding ubiquitin ligases; such enzymes could target
480 components of the Tpl2-regulated pathway. Protein phosphorylation and
481 ubiquitination are strongly linked in many signal transduction pathways to
482 control signalling and protein levels. As p53 undergoes complex post-
483 translational modifications including phosphorylation and ubiquitination [35],
484 one explanation is that decreased ubiquitination due to reduced ATF-2 activity
485 could drive increased p53 levels. Indeed, Tpl2 has been shown to regulate the
486 activity of the main p53 E3 ubiquitin ligase, HDM2 [30]. ATF-2 loss may activate
487 Tpl2 to reduce HDM2 activation or expression, allowing p53 to escape
488 proteasomal degradation and undergo nuclear accumulation. Furthermore,
489 both p21 and Cyclin D1 are also regulated by ubiquitination and proteolysis,
490 suggesting that ATF-2-regulated gene expression could have impact in this
491 context.

492 In conclusion, our study shows that in primary endothelial cells, basal and
493 ligand-activated signalling pathways are tightly regulated to ensure that signals
494 from the cytosol impact on nuclear gene expression and nuclear protein
495 function. A major finding is that a signalling axis involving Tpl2 serine/threonine
496 protein kinase and ATF-2 transcription factor with a wider impact on key cell
497 cycle regulators such as p53, p21 and Cyclin D1. This work also raises new
498 questions on the mechanisms of gene expression and the nature of post-
499 translational modifications that govern the levels of key cell cycle regulators.

500

501 **Conflict of interest**

502 The authors have no conflict of interest.

503

504 **Contributors**

505 G. W. Fearnley designed research, designed and performed
506 experiments, interpreted results, wrote and revised the manuscript. A. M.
507 Latham performed experiments and provided data. A. F. Odell designed
508 research, designed and performed experiments, interpreted results and
509 revised the manuscript. M. Hollstein helped to design experiments and carry
510 out the work. S. Ponnambalam designed research, interpreted results, wrote
511 and revised the manuscript.

512

513 **Acknowledgments**

514 We thank Annette Weninger for help with the qRT-PCR studies. We
515 thank the members of the Endothelial Cell Biology Unit for advice and support.
516 This work was supported by a grant from Yorkshire Cancer Research (AFO)
517 and Heart Research UK (TRP11/11).

518 **References**

- 519 [1] Proud CG, Cold Spring Harbor Persp Biol. 2019; 11:a033050.
- 520 [2] Lemmon MA, Schlessinger J, Cell. 2010;141:1117-1134.
- 521 [3] Lemmon MA, Freed DM, Schlessinger J, Kiyatkin A, Cell. 2016;164:1172-1184.
- 522 [4] Bates DO, Beazley-Long N, Benest AV, Ye X, Ved N, Hulse RP, Barratt S, Machado MJ,
523 Donaldson LF, Harper SJ, Peiris-Pages M, Tortonese DJ, Oltean S, Foster RR, Comp
524 Physiol. 2018;8:955-979.
- 525 [5] Apte RS, Chen DS, Ferrara N, Cell. 2019;176:1248-1264.
- 526 [6] Simons M, Gordon E, Claesson-Welsh L, Nat Rev Mol Cell Biol. 2016;17:611-625.
- 527 [7] Smith GA, Fearnley GW, Harrison MA, Tomlinson DC, Wheatcroft SB, Ponnambalam S,
528 J Inherit Metab Dis. 2015;38:753-763.
- 529 [8] Smith GA, Fearnley GW, Tomlinson DC, Harrison MA, Ponnambalam S, Biosci Rep.
530 2015;35:e00253.
- 531 [9] Fearnley GW, Smith GA, Odell AF, Latham AM, Wheatcroft SB, Harrison MA, Tomlinson
532 DC, Ponnambalam S, Meth Enzymol. 2014;535:265-292.
- 533 [10] Fearnley GW, Wheatcroft SB, Ponnambalam S, Meth Mol Biol. 2015;1332:49-65.
- 534 [11] Uhrig M, Ittrich C, Wiedmann V, Knyazev Y, Weninger A, Riemenschneider M,
535 Hartmann T, PLoS One. 2009;4:e6779.
- 536 [12] Ernst T, Hergenhausen M, Kenzelmann M, Cohen CD, Bonrouhi M, Weninger A, Klaren
537 R, Grone EF, Wiesel M, Gudemann C, Kuster J, Schott W, Staehler G, Kretzler M, Hollstein
538 M, Grone HJ, Am J Pathol. 2002;160:2169-2180.
- 539 [13] Sakaue-Sawano A, Kurokawa H, Morimura T, Hanyu A, Hama H, Osawa H, Kashiwagi
540 S, Fukami K, Miyata T, Miyoshi H, Imamura T, Ogawa M, Masai H, Miyawaki A, Cell.
541 2008;132:487-498.
- 542 [14] Wu LW, Mayo LD, Dunbar JD, Kessler KM, Baerwald MR, Jaffe EA, Wang D, Warren
543 RS, Donner DB, J Biol Chem. 2000;275:5096-5103.
- 544 [15] Fearnley GW, Odell AF, Latham AM, Mughal NA, Bruns AF, Burgoyne NJ, Homer-
545 Vanniasinkam S, Zachary IC, Hollstein MC, Wheatcroft SB, Ponnambalam S, Mol Biol Cell.
546 2014;25:2509-2521.
- 547 [16] Fearnley GW, Abdul-Zani I, Latham AM, Hollstein MC, Ladbury JE, Wheatcroft SB,
548 Odell AF, Ponnambalam S, Biol Open. 2019;8:bio034215.
- 549 [17] Fearnley GW, Bruns AF, Wheatcroft SB, Ponnambalam S, Biol Open. 2015;4:731-742.
- 550 [18] Klein EA, Assoian RK, J Cell Sci. 2008;121:3853-3857.
- 551 [19] Biegging KT, Mello SS, Attardi LD, Nat Rev Cancer. 2014;14:359-370.
- 552 [20] Engeland K, Cell Death Differ. 2018;25:114-132.
- 553 [21] Gkirtzimanaki K, Gkouskou KK, Oleksiewicz U, Nikolaidis G, Vyrla D, Lontos M,
554 Pelekanou V, Kanellis DC, Evangelou K, Stathopoulos EN, Field JK, Tsihliis PN, Gorgoulis
555 V, Liloglou T, Eliopoulos AG, Proc Natl Acad Sci USA. 2013;110:E1470-1479.
- 556 [22] Lee WJ, Lan KH, Chou CT, Yi YC, Chen WC, Pan HC, Peng YC, Wang KB, Chen YC,
557 Chao TH, Tien HR, Sheu WH, Sheu ML, Neoplasia. 2013;15:1036-1048.
- 558 [23] Dominguez-Brauer C, Brauer PM, Chen YJ, Pimkina J, Raychaudhuri P, Cell Cycle.
559 2010;9:86-89.

560 [24] Gordon EM, Ravicz JR, Liu S, Chawla SP, Hall FL, Mol Clin Oncol. 2018;9:115-134.
561 [25] Sakaue-Sawano A, Miyawaki A, Cold Spring Harbor Prot. 2014:pdb.prot080408.
562 [26] Chung AS, Ferrara N, Annu Rev Cell Dev Biol. 2011;27:563-584.
563 [27] Xu D, Matsumoto ML, McKenzie BS, Zarrin AA, Pharmacol Res. 2018;129:188-193.
564 [28] Johannessen CM, Boehm JS, Kim SY, Thomas SR, Wardwell L, Johnson LA, Emery
565 CM, Stransky N, Cogdill AP, Barretina J, Caponigro G, Hieronymus H, Murray RR, Salehi-
566 Ashtiani K, Hill DE, Vidal M, Zhao JJ, Yang X, Alkan O, Kim S, Harris JL, Wilson CJ, Myer
567 VE, Finan PM, Root DE, Roberts TM, Golub T, Flaherty KT, Dummer R, Weber BL, Sellers
568 WR, Schlegel R, Wargo JA, Hahn WC, Garraway LA, Nature. 2010;468:968-972.
569 [29] Kim G, Khanal P, Kim JY, Yun HJ, Lim SC, Shim JH, Choi HS, Mol Carcinogenesis.
570 2015;54:440-448.
571 [30] Lee JH, Lee JH, Lee SH, Do SI, Cho SD, Forslund O, Inn KS, Lee JS, Deng FM,
572 Melamed J, Jung JU, Jeong JH, Cancer Res. 2016;76:6712-6722.
573 [31] Lai DW, Lin KH, Sheu WH, Lee MR, Chen CY, Lee WJ, Hung YW, Shen CC, Chung
574 TJ, Liu SH, Sheu ML, Circ Res. 2017;121:e37-e52.
575 [32] Kanellis DC, Bursac S, Tsihchlis PN, Volarevic S, Eliopoulos AG, Oncogene.
576 2015;34:2516-2526.
577 [33] Roberts OL, Holmes K, Muller J, Cross DA, Cross MJ, J Cell Sci. 2010;123:3189-3200.
578 [34] Wang X, Gocek E, Novik V, Harrison JS, Danilenko M, Studzinski GP, Cell Cycle.
579 2010;9:4542-4551.
580 [35] Meek DW, Biochem J. 2015;469:325-346.
581
582

583 **FIGURE LEGENDS**

584 **Figure 1. VEGF-A-regulated gene expression exhibits dependence on**
585 **ATF-2 and p53.** (A) Endothelial cells subjected to treatment with siRNA
586 duplexes (scrambled or ATF-2) were treated under serum-free (SF), normal
587 growth media or VEGF-A₁₆₅ or VEGF-A₁₂₁ isoforms for 8 h followed by lysis and
588 immunoblotting (see Materials and Methods). Blots were probed using
589 antibodies specific for phospho-VEGFR2 (pY1175), VEGFR2, VCAM-1, ATF-
590 2, p21, actin, cyclins A2, B or D1. (B) Quantification of relative ATF-2 levels
591 after treatment with control (scrambled siRNA) or ATF-2 siRNA duplexes. (C)
592 Endothelial cells subjected to treatment with control untreated, scrambled,
593 ATF-2 and ATF-2/p53 combined siRNA duplexes were non-stimulated (-) or
594 treated with VEGF-A₁₆₅ or VEGF-A₁₂₁ isoforms (+) followed by lysis, and
595 immunoblotting with antibodies specific for phospho-VEGFR2, VEGFR2,
596 VCAM-1, p53, p21, phospho-ATF-2, ATF-2, cyclin D1 or tubulin. (D)
597 Quantification of relative levels of VCAM-1 levels in control, scrambled, ATF-2,
598 p53 and combined ATF-2/53 siRNA treatments under normal starvation
599 (control) or VEGF-A₁₆₅ isoform (165) stimulation. (E) Quantification of relative
600 p53 levels in control, scrambled, ATF-2, p53 and combined ATF-2/53 siRNA
601 treatments. (F) Quantification of relative levels of cyclin D1 levels after
602 treatment with control, scrambled, ATF-2, p53 and combined ATF-2/53 siRNA
603 duplexes. Error bars indicate \pm SEM ($n \geq 3$); significance is indicated by the
604 asterisks shown when $p < 0.05$ (*), $p < 0.01$ (**), $p < 0.001$ (***), $p < 0.0001$ (****).

605

606 **Figure 2. ATF-2 and Tpl2 regulate p53 and cyclin D1 levels in endothelial**
607 **cells.** (A) Endothelial cells subjected to treatment with control untreated,
608 scrambled, ATF-2 or combined ATF-2/p53 siRNA duplexes were lysed and
609 immunoblotted with antibodies specific for VEGFR2, p53, p21, Tpl2, phospho-
610 ATF-2, ATF-2, cyclin D1 and tubulin. (B, D, E) Quantification of relative protein
611 levels of (B) Tpl2, (D) p53, and (E) cyclin D1 after treatment with different

612 siRNA duplexes. (C) Quantification of relative *Tpl2* RNA levels after treatment
613 with control or ATF-2-specific siRNA duplexes. HUVECs treated with either
614 control scrambled siRNA or ATF-2-specific siRNA duplexes, serum starved for
615 2 h, stimulated with VEGF-A before lysis and qRT-PCR analysis (see Materials
616 and Methods). *Tpl2* RNA levels were normalised relative to control siRNA
617 treatment. (B-E) Error bars indicate \pm SEM ($n \geq 3$); significance is indicated by
618 the asterisks shown when $p < 0.05$ (*), $p < 0.01$ (**), $p < 0.001$ (***), $p < 0.0001$
619 (****).

620

621 **Figure 3. The endothelial cell cycle shows regulation by ATF-2, Tpl2 and**
622 **p53.** (A) Endothelial cells stably expressing the FUCCl reporter (see Materials
623 and Methods) were subjected to treatment with scrambled, ATF-2, p53 and
624 Tpl2 siRNA duplexes followed by synchronization and stimulation with 0.25 nM
625 VEGF-A₁₆₅ (VEGF-A) for 8 h or 30 h before fixation and visualization using
626 fluorescence microscopy. Quantification of endothelial cell populations after
627 treatment with scrambled, ATF-2, p53 and Tpl2, ATF-2/p53, ATF-2/Tpl2 siRNA
628 duplexes as shown in (B) G1/M, and (C) G0. (D) Quantification of endothelial
629 viability in cells subjected to treatment with control, scrambled or ATF-2 siRNA
630 duplexes. Error bars indicate \pm SEM ($n \geq 3$); significance is indicated by the
631 asterisks shown when $p < 0.05$ (*), $p < 0.01$ (**), $p < 0.001$ (***).

632

633 **Figure 4. ATF-2 levels influence endothelial cell apoptosis.** (A-D)
634 Endothelial cells were subjected to untreated control, scrambled, ATF-2, p53,
635 Tpl2, ATF-2/p53, ATF-2/Tpl2 siRNA duplexes before flow cytometry analysis
636 using combined propidium iodide and Annexin V-FITC staining (see Materials
637 and Methods). Quantification of (A) AnnexinV-labelled cell population, (B) early
638 apoptotic cells, (C) late apoptotic cells, and (D) total apoptotic cells after
639 treatment with different siRNA duplexes followed by flow cytometry. Error bars
640 indicate \pm SEM ($n \geq 3$); significance is indicated by the asterisks shown when

641 $p < 0.05$ (*), $p < 0.001$ (***). (E) Endothelial cells subjected to treatment with
642 scrambled or ATF-2-specific siRNA duplexes were lysed and immunoblotted
643 with antibodies specific for ATF-2, cleaved caspase 3, caspase 3, p53, Bax
644 and tubulin. (F) Quantification of relative levels of cleaved Caspase 3 in
645 endothelial cells subjected to treatment with scrambled or ATF-2-specific
646 siRNA duplexes. Error bars indicate \pm SEM ($n \geq 3$); significance is indicated by
647 the asterisks, $p < 0.01$ (**).

648

649 **Figure 5. ATF-2, Tpl2 and p53 levels modulate endothelial cell viability,**
650 **proliferation and tubulogenesis.** Quantification of endothelial cell (A)
651 viability, (B) proliferation, and (C) tubulogenesis after treatment with different
652 siRNA duplexes as indicated in each panel. In panel C, endothelial cells were
653 treated with different siRNA duplexes before assaying for tubulogenesis (see
654 Materials and Methods) by growth in normal medium (control) or VEGF- A_{165}
655 stimulated (165) tubulogenesis. In panels A-C, error bars indicate \pm SEM ($n \geq 3$);
656 significance is indicated by the asterisks shown when $p < 0.05$ (*), $p < 0.01$ (**),
657 $p < 0.001$ (***), $p < 0.0001$ (****). (D) Endothelial cells were treated with different
658 siRNA duplexes (scrambled, ATF-2, p53, Tpl2, ATF-2/p53, ATF-2/Tpl2) before
659 assaying for tubulogenesis. PECAM-1 staining was used for detecting
660 endothelial tubules using fluorescence microscopy (see Materials and
661 Methods). Bar, 1000 μ m.

662

663 **Figure 6. Regulation of endothelial cell cycle progression and apoptosis**
664 **by ATF-2, p53 and Tpl2.** (A) Under normal or steady-state conditions, the Tpl2
665 protein kinase maintains ATF-2 phosphorylation (Step 1) which negatively
666 regulates p53 levels, impacting on p21 and cyclin D1 expression (Step 2). ATF-
667 2 also negatively regulates Tpl2 levels. This translates into normal endothelial
668 cell cycle progression and function (Step 3). (B) Under conditions of reduced
669 ATF-2 activity or levels there is a rise in Tpl2 levels (Step 4) which positively

670 regulates p53 levels, impacting on p21 and cyclin D1 expression (Step 5). This
671 translates into cell cycle arrest and apoptosis (Step 6).

Figure 1

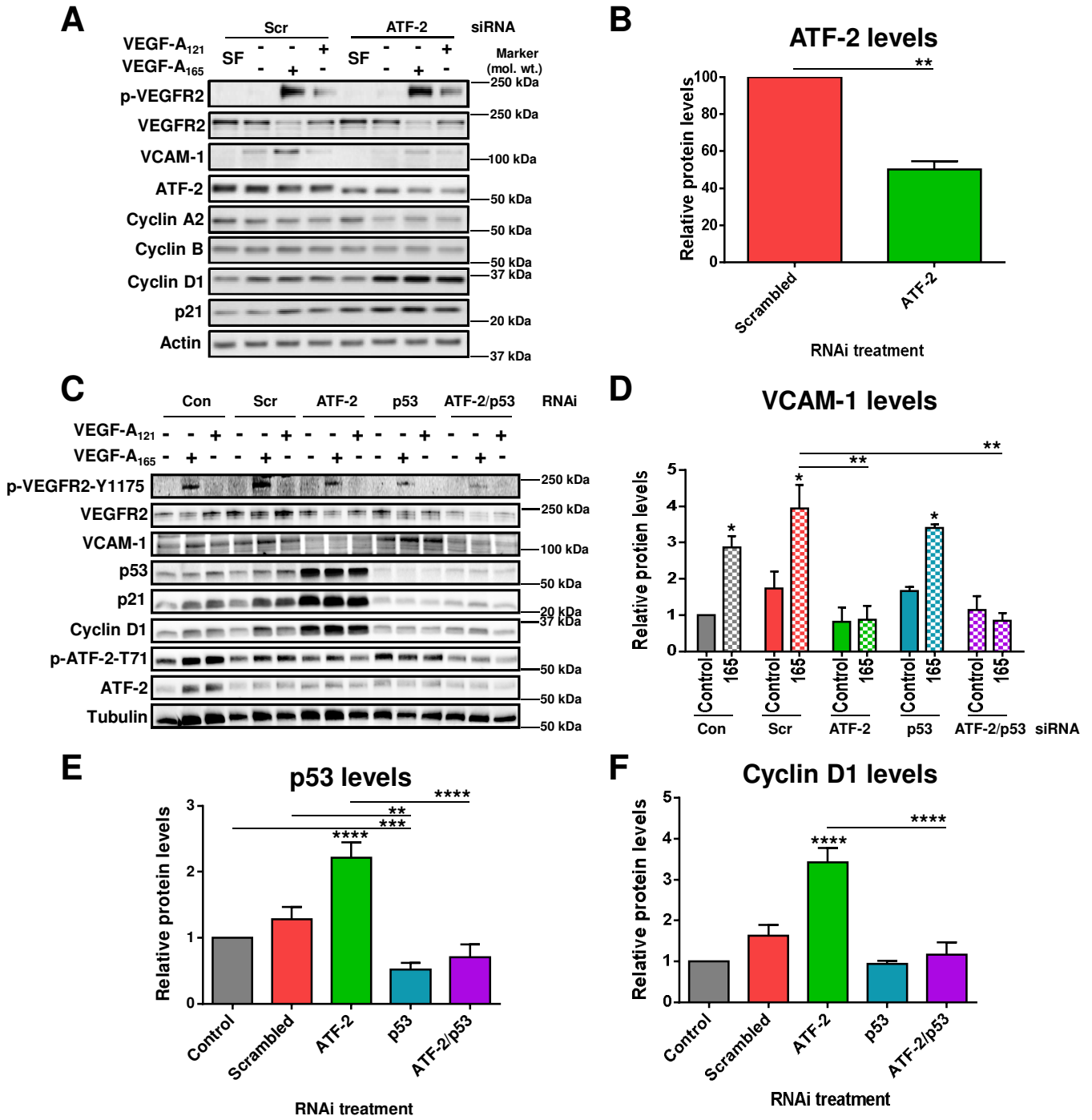


Figure 2

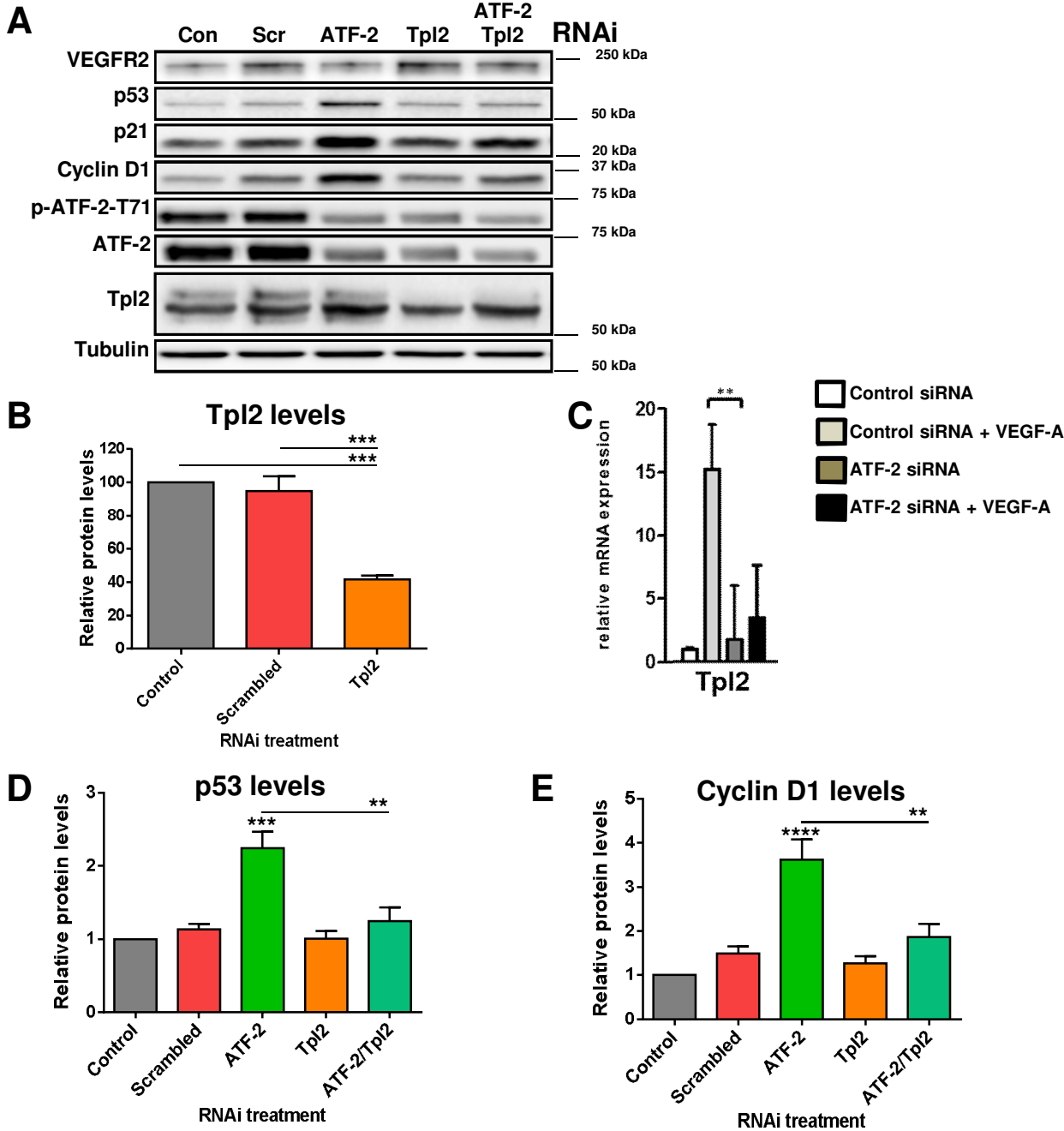


Figure 3

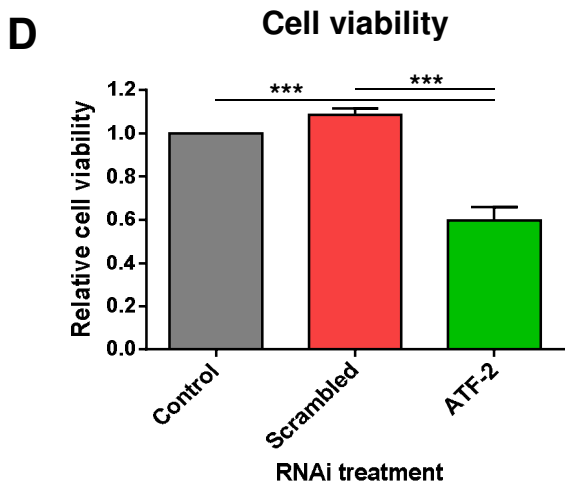
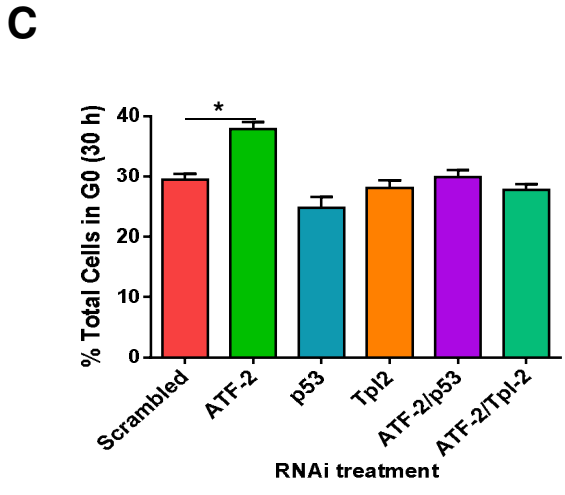
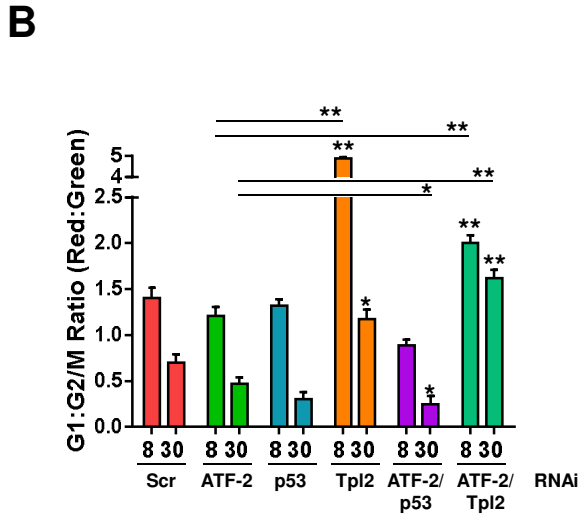
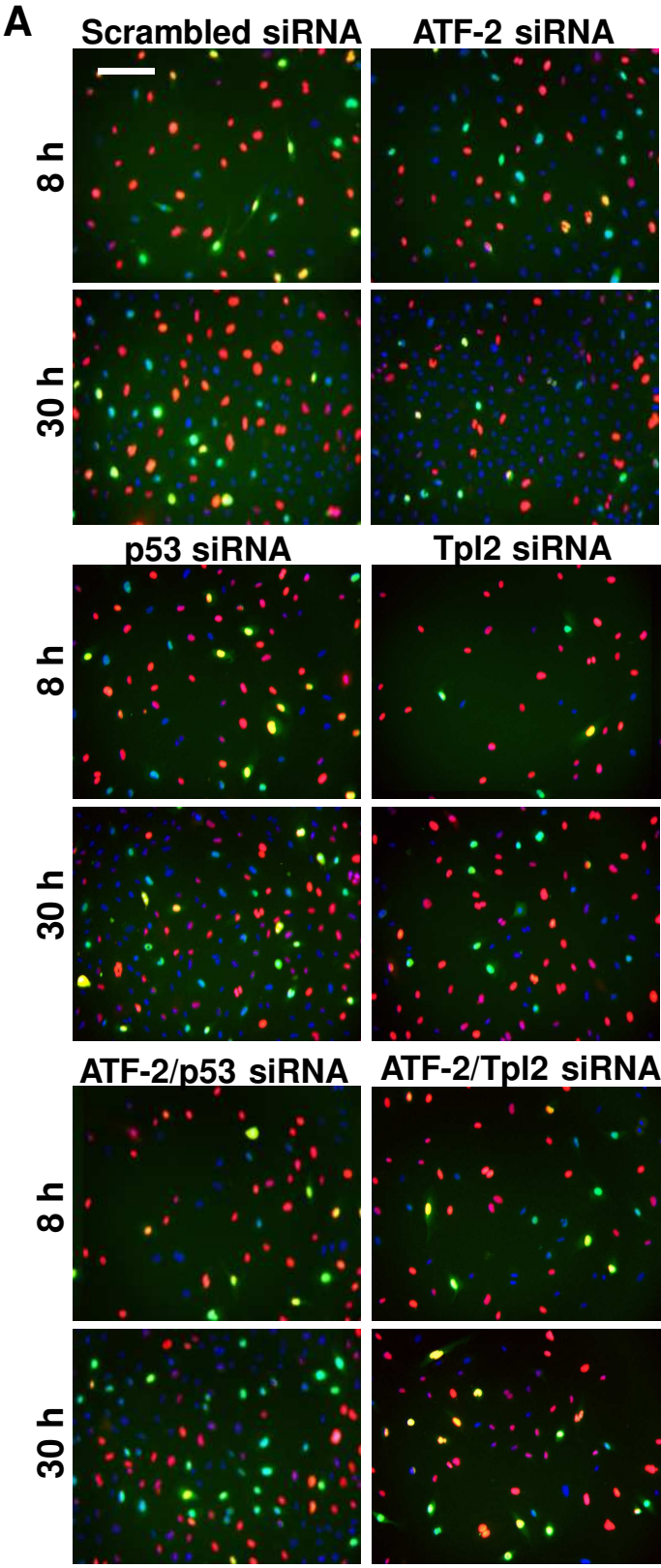


Figure 4

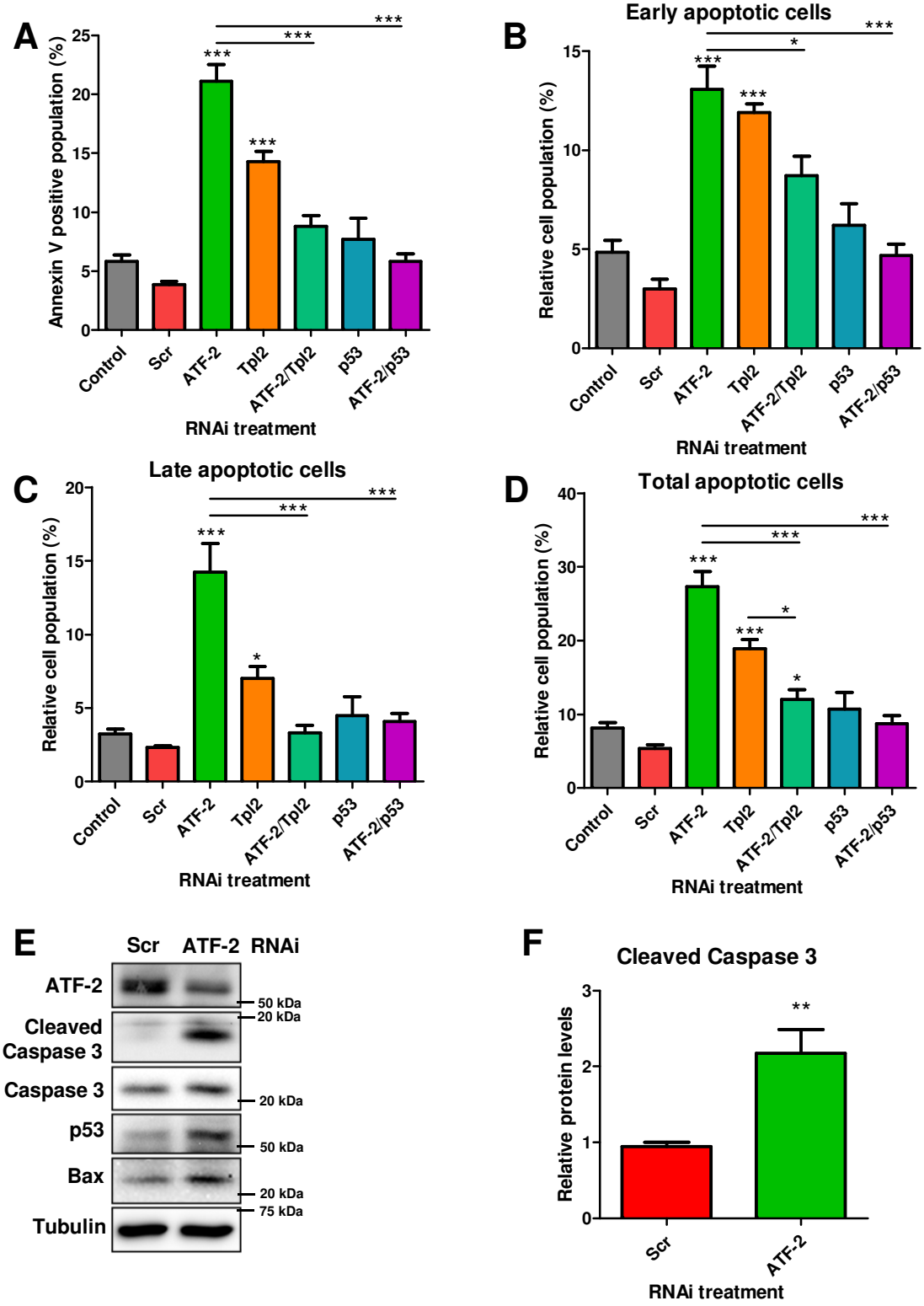


Figure 5

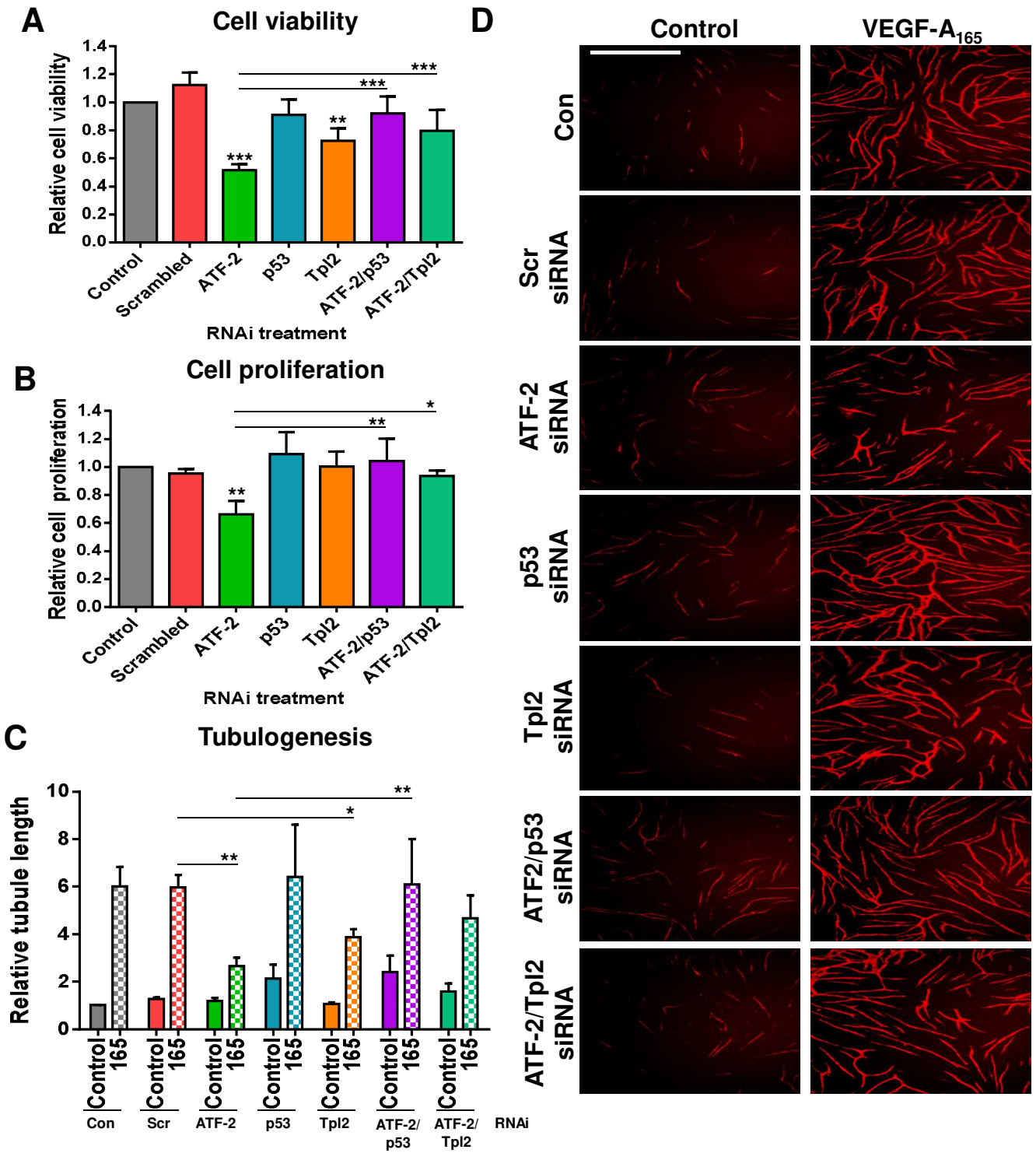
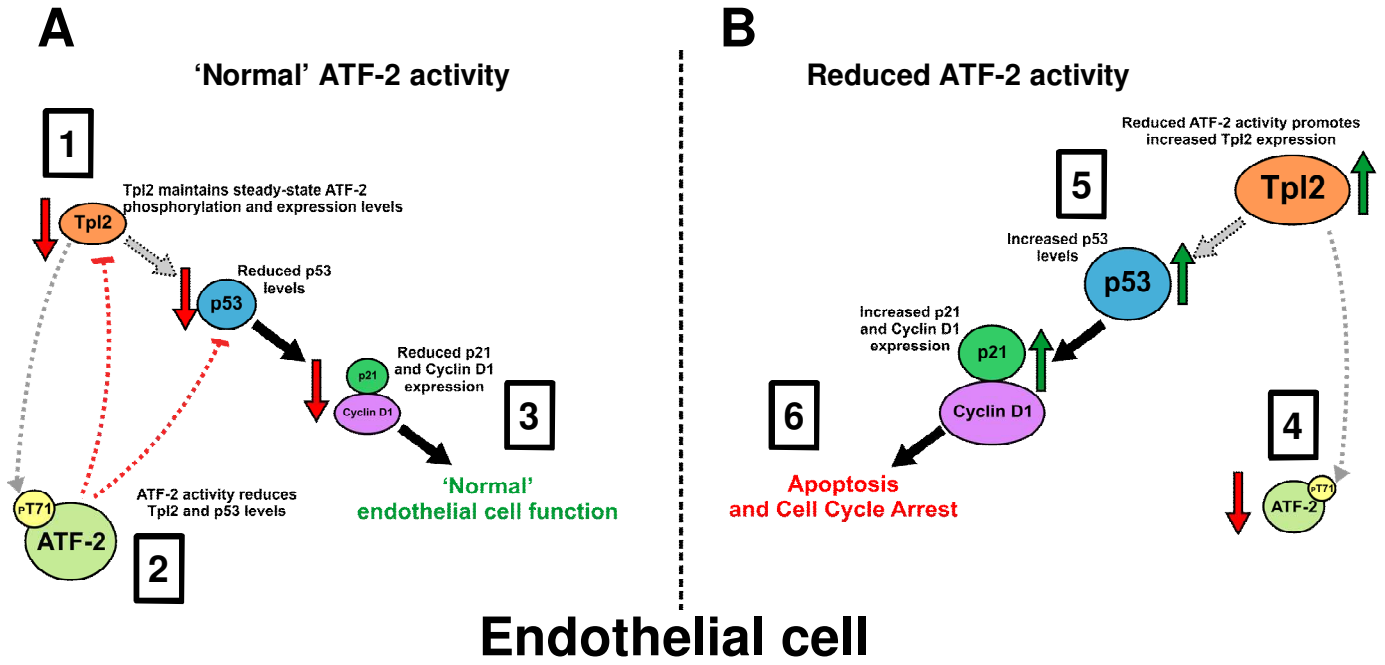


Figure 6



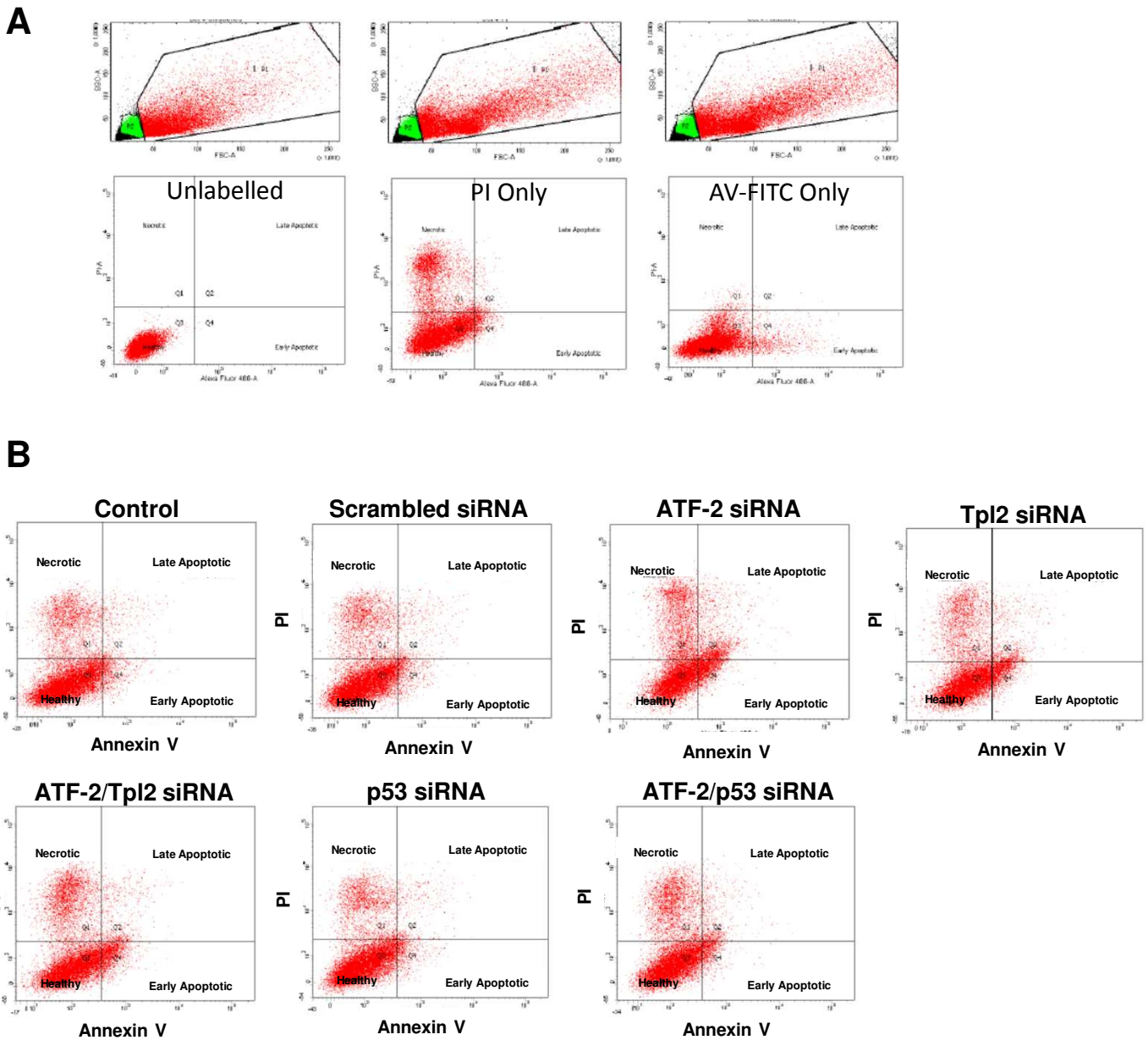


Figure S1. Flow cytometry analysis of endothelial cell apoptosis. (A) Control untreated endothelial cells were subjected to no labelling or with either propidium iodide (PI) or AnnexinV-FITV (AV-FITC). (B) Endothelial cells subjected to treatments using scrambled, ATF-2, p53, Tpl2, ATF-2/p53, ATF-2/Tpl2 siRNA duplexes before flow cytometry analysis using combined propidium iodide and Annexin V-FITC staining (see Materials and Methods). The different cell populations (healthy, necrotic, early apoptotic and late apoptotic) are indicated in each quadrant.